

Can Southern Ocean Eddy Effects Be Parameterized in Climate Models?

FRANK O. BRYAN, PETER R. GENT, AND ROBERT TOMAS

National Center for Atmospheric Research, Boulder, Colorado

(Manuscript received 26 October 2012, in final form 3 July 2013)

ABSTRACT

Present-day control and 1% yr⁻¹ increasing carbon dioxide runs have been made using two versions of the Community Climate System Model, version 3.5. One uses the standard versions of the ocean and sea ice components where the horizontal resolution is 1° and the effects of mesoscale eddies are parameterized, and the second uses a resolution of 1/10° where the eddies are resolved. This is the first time the parameterization has been tested in a climate change run compared to an eddy-resolving run. The comparison is made not straightforward by the fact that the two control run climates are not the same, especially in their sea ice distributions. The focus is on the Antarctic Circumpolar Current region, where the effects of eddies are of leading order. The conclusions are that many of the differences in the two carbon dioxide transient forcing runs can be explained by the different control run sea ice distributions around Antarctica, but there are some quantitative differences in the meridional overturning circulation, poleward heat transport, and zonally averaged heat uptake when the eddies are parameterized rather than resolved.

1. Introduction

Nearly all projections of future change made with climate models have used an ocean component that has non-eddy-resolving horizontal resolution of about 1° or coarser. Since the late 1990s, the large majority of these ocean components have used the Gent and McWilliams (1990) parameterization to represent the effects of mesoscale eddies on the mean flow. A question that has frequently been raised is: Does this parameterization give the correct ocean response in climate change scenario runs? Examples are Soloviev et al. (2002), Hallberg and Gnanadesikan (2006), and a recent review paper on the Southern Ocean by Marshall and Speer (2012). Marshall and Speer write, “The emerging link between upwelling and mesoscale eddy fluxes places a large burden on climate models as the relatively small-scale eddy fluxes are computationally difficult to obtain and their parameterizations may not always be faithful, especially in a changing climate.” In this paper, aspects of this important question are addressed for the first time. We compare results from an idealized future climate scenario using two versions of a climate model that uses

different ocean components where the horizontal resolution is non-eddy resolving and eddy resolving.

As computer power has increased over the past decade, many basin- to global-scale ocean-alone simulations using eddy-resolving horizontal resolution of 0.1° or finer have been performed. While they are not totally numerically converged in the sense that the solutions are independent of the resolution, there is no doubt that this resolution gives a much more realistic representation of mesoscale eddies and strong currents (and matches global satellite observations of sea surface height variability) than when coarser resolution is used (see Bryan et al. 2007). However, the computational cost of eddy-resolving resolution is so high that coupled climate model runs with resolved eddies have only recently been attempted, and they are relatively short integrations (McClellan et al. 2011; Kirtman et al. 2012). Some climate centers have used their increased computer power to run versions where the ocean resolution is in the range between 0.5° and 0.25°, which is known as eddy permitting because the sea surface height variability does not match satellite observations. When eddy permitting, the ocean component may or may not use an eddy parameterization, but the mesoscale eddies are not fully resolved. Very recently, Delworth et al. (2012) showed results from the Geophysical Fluid Dynamics Laboratory (GFDL) Climate Model, version 2.5

Corresponding author address: Frank O. Bryan, NCAR, P.O. Box 3000, Boulder, CO 80307.
E-mail: bryan@ucar.edu

(CM2.5), where the ocean component's resolution is 0.25° and no eddy parameterization is used. Results from the CM2.5 transient forcing run where carbon dioxide is increased by $1\% \text{ yr}^{-1}$ are compared to results using the CM2.1, where the ocean component uses 1° resolution.

Also over the past decade, improvements to the implementation of the Gent and McWilliams (1990) parameterization (GM) have been made. These include several proposals of how to calculate the GM coefficient from model variables so that it varies in space to mimic the spatial variation of eddy kinetic energy observed in the ocean. Eddy kinetic energy is high in the western boundary currents and in other locations such as the Antarctic Circumpolar Current (ACC). It has recently been shown that using a variable coefficient is important so that climate models can respond in the same way to increased Southern Hemisphere zonal winds as eddy-resolving and eddy-permitting ocean models such as Hogg et al. (2008), Screen et al. (2009), and Spence et al. (2010). These high-resolution models respond to wind changes over the ACC by changes in eddy activity such that the meridional overturning circulation (MOC) due to the eddies compensates in large part for the directly wind-forced changes in the mean flow MOC. Results showing this partial eddy compensation to changed zonal winds have been published using a modified version of the GFDL CM2.1 (Farneti and Gent 2011), and using the Community Climate System Model, version 4 (CCSM4; Gent and Danabasoglu 2011). This work uses the same variable GM coefficient implementation as in the CCSM4, which is documented in Danabasoglu et al. (2012).

In this study, we compare very similar control and transient carbon dioxide forcing runs as in Delworth et al. (2012), but with a horizontal resolution in the ocean component of 5.5 km at the latitude of Drake Passage. Here, the Rossby radius of deformation is approximately 10 km (Chelton et al. 1998), so we are able to explicitly resolve a considerably larger fraction of the energetic scales. A comparison with the Delworth et al. (2012) results is made below in section 5. The layout of the paper is as follows: Section 2 documents the two model versions used, and the experiments performed. Section 3 shows results from the two present-day control runs, and section 4 contains results from the two transient forcing runs. Discussion of the results is presented in section 5, and the conclusions are given in section 6.

2. The models and experiments

The two model versions used in this study are variants of the CCSM. They use CCSM, version 3.5, which is an interim configuration on the way to CCSM4 that is

documented in Gent et al. (2011). Version 3.5 contained a large majority of the improvements made in completing CCSM4, and these improvements are listed in Gent et al. (2010). Gent et al. (2010) show results using exactly the same model configuration as what is labeled the low-resolution (LR) model version in this study, although the runs analyzed are different. The atmosphere component has a horizontal resolution of $0.47^\circ \times 0.63^\circ$ using the Lin–Rood finite-volume dynamical core (Lin 2004) and has 26 levels in the vertical. The atmosphere includes the changes to the deep convection scheme that resulted in the significant improvement to the simulated ENSO frequency described in Neale et al. (2008) and Gent et al. (2011). In addition, the increased (nominally 0.5°) horizontal resolution has stronger winds located nearer to the coast in major upwelling regions, which leads to much reduced sea surface temperature (SST) biases in those regions (Gent et al. 2010). The land component is run on the same grid as the atmosphere, and the version used is documented in Oleson et al. (2008).

The ocean component in the LR setup uses the standard nominal 1° , non-eddy-resolving horizontal resolution used in CCSM4. The zonal resolution is uniformly 1.12° , and the meridional resolution is 0.27° at the equator gradually increasing to 0.54° at 33° latitude and constant at higher latitudes. In the Northern Hemisphere, the grid is transformed so that the grid pole is in Greenland at 80°N , 40°W . The vertical resolution is uniformly 10 m in the upper 200 m , and then increases with depth, and there are 60 levels in total. The formulation of the eddy parameterization from Gent and McWilliams (1990) near the surface follows the form described in Danabasoglu et al. (2008). The GM coefficient is now a function of space and time following the implementation in Danabasoglu and Marshall (2007) and decreases with depth varying as the square of the local buoyancy frequency. The advection scheme is a flux-limited Lax–Wendroff form that is less diffusive than the standard third-order upwind scheme. The ocean component does not include the parameterizations of overflows and effects of submesoscale eddies that are part of the released CCSM4 code (Danabasoglu et al. 2012). The sea ice component runs on the same grid as the ocean component, and is based on the Community Ice Code (CICE), version 4. It has most of the improvements in the CCSM4 version documented in Holland et al. (2012), but does not have the aerosol or black carbon parameterizations.

The high-resolution (HR) model version in this study uses exactly the same nominal 0.5° -resolution version of the atmosphere and land components, but much higher horizontal resolution in the ocean and sea ice components. The resolution is 0.1° in the zonal direction and

$0.1^\circ \times \cos(\text{latitude})$ in the meridional direction, which has been shown to be adequate for reproducing satellite-observed sea surface height variability, and is the minimum resolution sufficient to be referred to as eddy resolving (Smith et al. 2000). In the Northern Hemisphere, the ocean uses a tripole grid with grid poles in Canada and Russia, which keeps the resolution and grid aspect ratio fairly uniform in the high northern latitudes. In this version, the GM eddy parameterization is not used, and is replaced by a horizontal biharmonic diffusion, and the viscosity is also a biharmonic formulation. The biharmonic coefficients vary spatially with the cube of the average grid length. Previous studies using this, or a very similar, configuration of this ocean component are described in Maltrud et al. (2010), Bryan et al. (2010), McClean et al. (2011), Kirtman et al. (2012), and Bitz and Polvani (2012). Additional differences with the LR ocean component are that only 42 levels are used in the vertical, the advection scheme is second order centered, and partial bottom cells are used in the specification of the bottom topography: partial cells are not used in the LR ocean model. These differences complicate the interpretation of the results, but cause much smaller differences than the difference between mesoscale eddies being resolved or not. In the HR version, the sea ice component is also run on the same 0.1° grid as the ocean component and includes the improvements for use at high resolution described in Lipscomb et al. (2007). No tuning of the many parameter values in this climate model was done for the HR run, so that, apart from the differences described in this paragraph, the HR version uses the same parameter values as the LR version.

The initial conditions for the ocean and sea ice components in the LR run are described in Kirtman et al. (2012), and are taken from the end of a previous present-day control run of the CCSM3. The idea was to use a model state that had been integrated long enough so that the ocean above about 2 km had come into equilibrium. However, all the components of CCSM3.5 had been upgraded from CCSM3, so that an initial shock at the start of the integration was inevitable. The initial conditions for the ocean and sea ice components in the HR run were the same as in the LR run, but interpolated to the much finer horizontal grid in that run. Both of these present-day control runs used a constant globally averaged carbon dioxide (CO_2) mixing ratio of 355 ppmv, which is its measured value in 1990. Both control runs were integrated for 167 yr, which in the case of the HR run took several months to complete. Note that 167 yr is not a long control run, but it was decided to integrate the LR run for the same length of time as the HR run, given that they both started with the same initial conditions.

The 1% increasing CO_2 runs in both the LR and HR versions start from the beginning of year 77 of the respective control runs. The CO_2 mixing ratio in the atmosphere component is increased by $1\% \text{ yr}^{-1}$ until the start of year 147, when it has doubled from its initial value. Both transient forcing runs are then integrated until the end of year 167 with the CO_2 mixing ratio kept constant at its doubled value. Again, the HR transient forcing run took several months to complete. In the following sections, model results are shown that are averages over years 147–167 from both the present-day control ($1 \times \text{CO}_2$) and transient forcing ($2 \times \text{CO}_2$) LR and HR integrations.

A thorough comparison of the mean climates and their variability from the LR and HR control runs is presented in Kirtman et al. (2012). Their Fig. 3 shows that the North Atlantic and Arctic Ocean SSTs are 2° – 5°C warmer in HR than LR. The Arctic sea ice concentrations in March and September from the two control runs are shown in Fig. 14 of Kirtman et al. (2012). The LR simulation is quite realistic, similar to the CCSM4 simulation shown in Gent et al. (2011), and reflects the fact that the climate model parameters have been tuned to give realistic results at low resolution. The HR control run has a significantly poorer simulation, with the Arctic sea ice being much too thin and it has almost no sea ice in September compared to observations. However, no tuning of the HR parameters was possible, because the huge computational resource required by this version eliminates the possibility of multiple control runs. This large difference between the mean Arctic sea ice simulations in LR and HR has a very big impact on the Arctic response in the CO_2 transient forcing runs. After CO_2 doubling, the LR increase in atmospheric surface temperature is $<6^\circ\text{C}$ virtually everywhere in the Arctic, whereas the HR has a $>6^\circ\text{C}$ increase over a significant area. In the HR, all of the too thin Arctic ice melts away during the summer under $2 \times \text{CO}_2$, whereas there is still considerable ice cover in the LR. This allows the HR Arctic SSTs to warm considerably, and so does the surface atmospheric temperature.

3. Control run results

The Antarctic sea ice distributions in the LR and HR control runs are much more similar than are the Arctic distributions. In addition, it is well known that the effect of ocean mesoscale eddies is of leading-order importance on the temperature, salinity, and density distributions across the ACC. Thus, if the GM eddy parameterization is going to have trouble mimicking the effects of resolved eddies, then that will have its largest implications in the ACC region. Therefore, the analysis of the LR

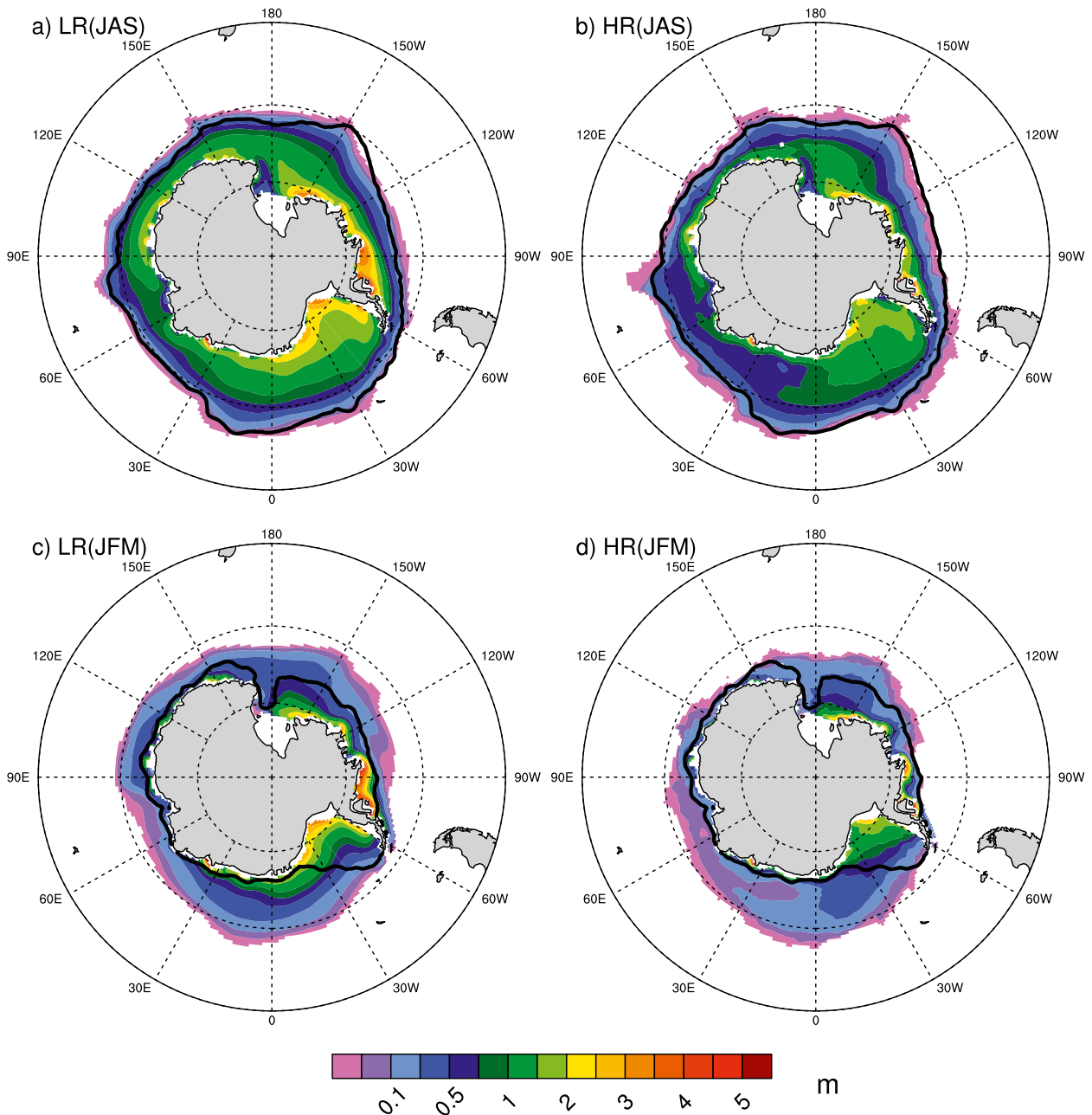


FIG. 1. The mean Antarctic sea ice thickness (m) in austral winter (JAS) in the (a) LR and (b) HR control simulations and in austral summer (JFM) in the (c) LR and (d) HR control runs. The solid black line is the 15% concentration contour from SSM/I observations.

and HR control and CO_2 transient forcing runs will concentrate on the Southern Hemisphere, the Southern Ocean, and on the change in Antarctic sea ice distributions.

Figure 1 shows the average Antarctic sea ice thickness in austral winter [July–September (JAS)] and summer [January–March (JFM)] from years 147 to 167 of the two control runs. In winter, the ice extent is similar, but the HR has a slightly smaller extent in the Pacific sector.

There is more contrast in the ice thickness, with the LR having more ice over 1-m thick, and thicker ice near the continent in the Atlantic and Pacific sectors. There is a larger difference in the summer sea ice extents, with the ice retreating somewhat farther south in the HR run making it compare better with the solid black line, which is the 15% concentration contour from the Special Sensor Microwave Imager (SSM/I) observations. The ice thickness is also simulated better in the HR, with most of the

TABLE 1. Antarctic sea ice volume (10^{13} m^3).

Model	Run	Mean	Std dev
LR	$1 \times \text{CO}_2$	1.578	0.131
HR	$1 \times \text{CO}_2$	1.083	0.058
LR	$2 \times \text{CO}_2$	0.940	0.085
HR	$2 \times \text{CO}_2$	0.786	0.094

ice being less than 1-m thick. Thus, the annual cycle in Antarctic sea ice volume is captured better in HR. The mean volume of Antarctic sea ice for LR is $1.58 \times 10^{13} \text{ m}^3$, which is 46% higher than the HR mean volume of $1.08 \times 10^{13} \text{ m}^3$ (see Table 1).

A possible reason for the different sea ice distributions in both hemispheres is different LR and HR poleward ocean heat transports, and Fig. 2 shows the zonally integrated northward heat transport from the end of the two control runs. Also plotted are the contributions to the total transports by the mean flow and mesoscale eddies, which are calculated as follows. In both LR and HR, the mean annual cycle of temperature and velocity over years 147–167 was calculated and added to the 21-yr time mean. The eddies are then defined as the difference between the instantaneous flow and this calculated time mean plus annual cycle. Thus, the “mean” contribution in Fig. 2 is due to the time mean plus annual cycle, and the “eddy” contribution is due to parameterized or resolved mesoscale eddies plus the heat transport by interannual variability, such as El Niño–Southern Oscillation (ENSO).

Figure 2 also shows that poleward of 50°N , HR has considerably more poleward heat transport than does LR. This increase is all in the mean flow transport, because the eddies in both runs cause very little heat transport north of 50°N . There is almost no change in the global atmospheric heat transport in the LR and HR runs, because they use the same atmosphere component at the same resolution. Mahlstein and Knutti (2011) analyze results from 22 climate models in phase 3 of the Coupled Model Intercomparison Project (CMIP3) archive. Mahlstein and Knutti’s Fig. 6 shows that there is a strong negative correlation between the ocean northward heat transport at 60°N and the Arctic sea ice extent over years 1970–99 in these models. Therefore, the considerably larger HR total ocean heat transport in the high latitudes of the Northern Hemisphere is consistent with the much-reduced Arctic sea ice volume in HR compared to LR. In the high latitudes of the Southern Hemisphere, the LR and HR transports are more similar, with the LR transporting more heat southward across the ACC between 50° and 60°S , but with HR transporting fractionally more heat south of 64°S . Note that the LR southward eddy transport is consistently

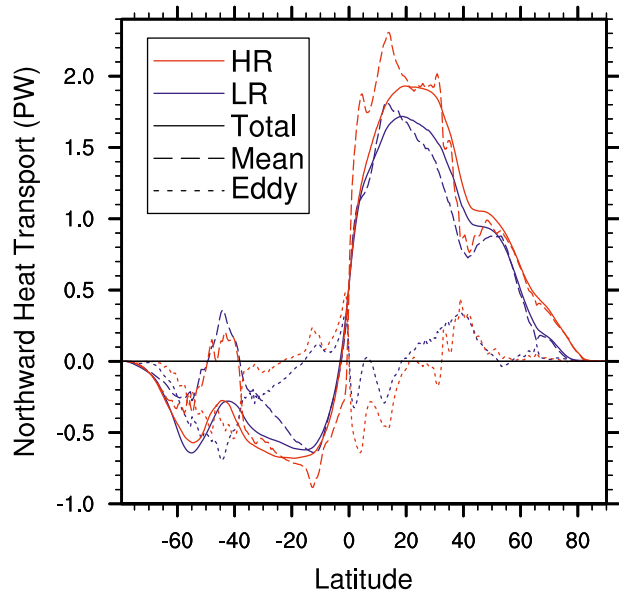


FIG. 2. The mean total northward ocean heat transport (PW) in the LR and HR control runs. The total transport (solid lines) is divided into the mean flow (long dashed lines) and eddy flow (short dashed lines) contributions.

larger than the HR eddy transport south of 45°S , which includes the latitudes of the ACC. South of 64°S , the LR mean transport is smaller than the HR mean transport, which partially offsets the larger LR eddy transport. Again, the fractionally larger HR southward heat transport south of 64°S is consistent with the smaller Antarctic sea ice volume for HR than LR.

4. Doubled CO_2 run results

Results will be shown from years 147 to 167 of the CO_2 $1\% \text{ yr}^{-1}$ transient forcing runs when the CO_2 mixing ratio was doubled and compared to results from the same years of the control runs. Figure 3 shows the difference in atmospheric surface temperature south of 30°S between $2 \times \text{CO}_2$ and $1 \times \text{CO}_2$ for the LR and HR versions. The globally averaged surface temperature increases are very similar: 1.68°C for LR and 1.71°C for HR. Figure 3 shows that the changes in atmospheric surface temperature, which over the oceans is the same as SST, are quite similar. The surface temperature increase over the ocean is about 1°C , although there are larger areas in the South Pacific in HR where the change is $<1^\circ\text{C}$ than in LR. The LR has larger areas off the coast of Antarctica where the increase is $>4^\circ\text{C}$ than does the HR, and this is related to the fact that the LR loses more sea ice in these regions than does the HR.

Figure 4 shows time series of Antarctic ice volume for $2 \times \text{CO}_2$ and $1 \times \text{CO}_2$ from the LR and HR. As shown in

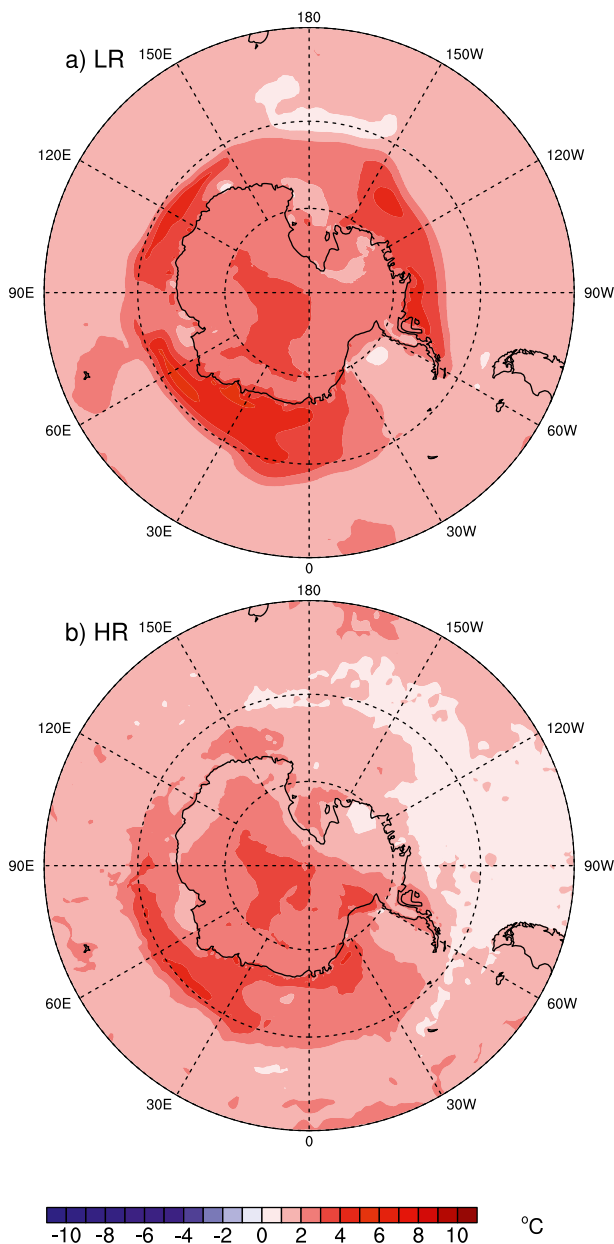


FIG. 3. The difference in atmosphere surface temperature ($^{\circ}\text{C}$) south of 30°S between $2 \times \text{CO}_2$ and $1 \times \text{CO}_2$ in (a) LR and (b) HR.

Fig. 1, the LR control has somewhat more ice than the HR, but Fig. 4 and Table 1 show there is considerable interannual variability in the ice volume in all four runs. The means and standard deviations of Antarctic annual mean ice volume are listed in Table 1, which shows that the mean ice volume has decreased by 40% in LR but by only 26% in HR. Despite the quite large standard deviations, this difference in mean ice decrease is significant at the 99% level using a two-sided Student's t test, where the effective number of degrees of freedom is

reduced from 21 based on the usual method of using lag-one autocorrelations. Figure 5 shows the changes in mean sea ice thickness in winter (JAS) and summer (JFM) from the LR and HR. The LR ice thins everywhere, and the larger volume loss is not because the LR ice extent decreases much more than the HR. Comparison with Fig. 1 shows the LR loses more ice than HR where the LR control run ice is considerably thicker than the HR, which can be explained as a basic property of sea ice thermodynamics; see the discussion in the next section.

Figures 6a and 6b are the zonally averaged annual zonal wind stress between 30° and 80°S from $2 \times \text{CO}_2$ and $1 \times \text{CO}_2$ for the LR and HR, and show that the maximum zonal wind stress value increases by 3%–4% in $2 \times \text{CO}_2$ for both models. Even though the maxima remain at the same latitude, the region of largest wind stress moved a degree or so to the south under $2 \times \text{CO}_2$ for both models. The largest difference between the models is the wind stress change in winter, which is shown in Figs. 6c and 6d. In LR there is almost no change in the maximum wind stress value, in contrast to an increase of about 5% in the HR stress maximum for $2 \times \text{CO}_2$ shown in Fig. 6d. The changes in zonal wind stress maximum strength and position will have an effect on the magnitude and latitude of the Southern Ocean mean flow MOC maximum.

Figures 7a and 7b show the changes in the mean zonally integrated global MOC between 30° and 80°S for LR and HR. The dipole patterns show that the large MOC in the Southern Ocean has increased and moved slightly to the south, in response to the increase and small southward shift in the zonal wind stresses shown in Figs. 6a and 6b. Even though the maximum MOC changes are very similar, there are differences between the LR and HR MOC changes. The positive change between 50° and 70°S reaches deeper for HR, down to almost 5 km. Also, the negative values north of 50°S are confined to the upper ocean for LR, but reach deeper into the ocean for HR. Figures 7c and 7d show the changes in the LR MOC of the total flow and eddy-induced flow resulting from the GM parameterization. In the Southern Ocean, and especially across the ACC, the eddy-induced MOC acts to flatten the isopycnals and so opposes the mean flow MOC that is acting to steepen them. Comparison of Figs. 7a and 7d shows that the eddy-induced MOC change does oppose the mean flow MOC change in the upper 2 km between 30° and 50°S , and throughout the ocean depth in a narrow band around 60°S . However, across much of the ACC between 50° and 60°S , the eddy-induced MOC change strengthens the mean flow MOC change. This indicates that MOC changes are not just because of the changes

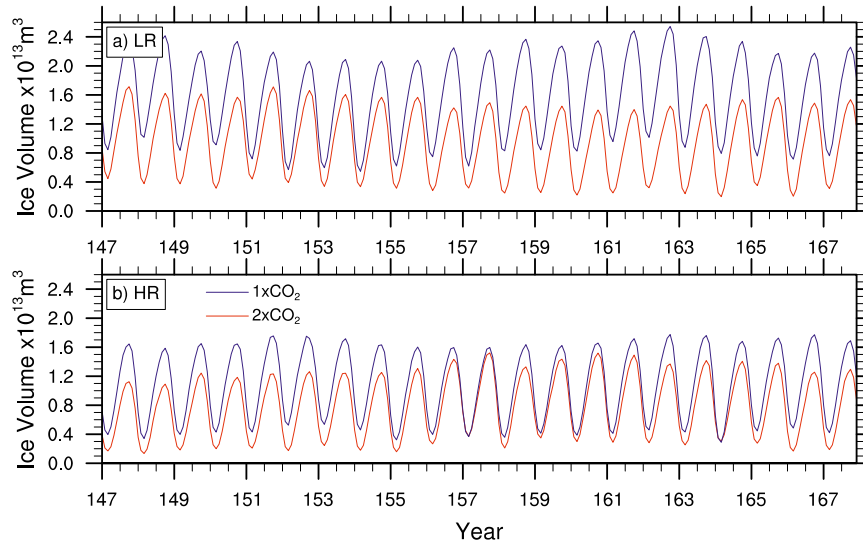


FIG. 4. Time series over years 147–167 of Antarctic sea ice volume (10^{13} m^3) for $2 \times \text{CO}_2$ and $1 \times \text{CO}_2$ in (a) LR and (b) HR.

in the wind stress shown in Fig. 6, but are also because of the changes in the temperature distributions shown below, and further discussion of this point is presented in the next section. Unfortunately, the HR eddy MOC change is not available to compare with Fig. 7d because the correlations between the velocity and thickness fields were not calculated during the runs, and only monthly output was archived.

Figure 8 shows the change in zonally averaged ocean temperature between $2 \times \text{CO}_2$ and $1 \times \text{CO}_2$ over 30° – 80°S for LR and HR. The temperature change near the surface is very close in the two versions, both having a maximum increase of 1.4°C near 45°S at 50-m depth. The reason for the increase at this latitude, which reaches deeper into the ocean than at adjacent latitudes, is a stronger Ekman convergence in $2 \times \text{CO}_2$ as a result of the stronger mean surface Ekman flow south of 45°S , but weaker surface Ekman flow north of 45°S , as shown in Figs. 7a and 7b. The temperature change north of 62°S , which includes the ACC latitudes, is very similar in depth, with a warming greater than 0.4°C down to nearly 1-km depth. The warming of $>0.2^\circ\text{C}$ does reach a little deeper for LR than HR between 40° and 50°S . The total heat uptake in the upper kilometer of the Southern Hemisphere oceans in $2 \times \text{CO}_2$ compared to $1 \times \text{CO}_2$ is $4.0 \times 10^{23} \text{ J}$ for HR compared to $3.7 \times 10^{23} \text{ J}$ for LR. There are larger differences in the deeper ocean south of 62°S , with the HR having a somewhat larger volume where the temperature change is $>0.1^\circ\text{C}$, which reaches to the bottom and spreads northward to 45°S . The additional heat uptake in $2 \times \text{CO}_2$ below 1 km is $1.3 \times 10^{23} \text{ J}$ for HR compared to $0.6 \times 10^{23} \text{ J}$ for LR.

This larger heat uptake is probably related to the thinner, more realistic Antarctic sea ice distribution, especially in summer, in the HR control run, where the 0.1° resolution allows the simulation of realistic open-water polynyas.

Figure 9 shows the change in total northward heat transport between $2 \times \text{CO}_2$ and $1 \times \text{CO}_2$ over 30° – 80°S for LR and HR, plus its division into mean and transient eddy components, and the solid lines represent the mean values over years 147–167. The eddy component changes are very small south of 45°S , so the question arises as to whether they are significant. The runs do not extend beyond year 167, so a standard deviation cannot be calculated by using results from many 21-yr segments. Therefore, an estimate of the standard deviation is calculated by following the bootstrap-type method described in section 5.3.2 of Wilks (1995). A different estimate is constructed by randomly drawing 21 times a year from 147 to 167. Thus, some years from 147 to 167 can appear multiple times in an estimate, and other years do not appear at all. This is done 50 times, and the different total, mean, and eddy northward heat transports are then calculated from each estimate. The standard deviations of the three transports are calculated as a function of latitude from these 50 estimates, and shown by the shading in Fig. 9. The total southward heat transport is reduced everywhere south of 30°S for both LR and HR, with a similar dependence on latitude. The maximum reduction at 50°S is 0.17 PW for LR, compared to the larger change of 0.20 PW for HR, and the change is significant at all latitudes for both models. Around 40°S , there is a somewhat larger change in the

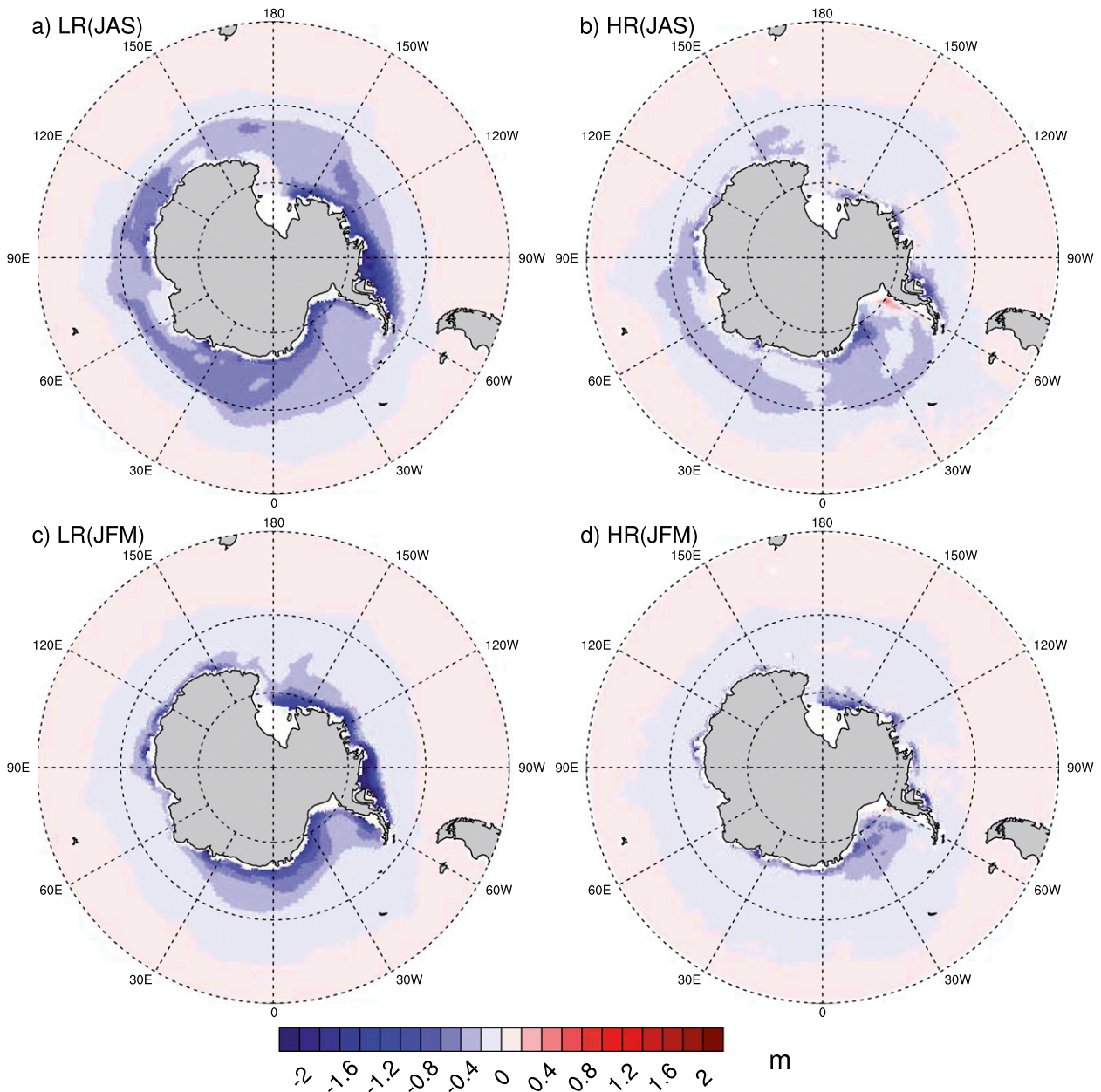


FIG. 5. Change in mean Antarctic sea ice thickness (m) between $2 \times \text{CO}_2$ and $1 \times \text{CO}_2$ in austral winter (JAS) for (a) LR and (b) HR and in austral summer (JFM) for (c) LR and (d) HR.

eddy transport for HR than LR and the mean transport changes are very small and of opposite sign, but the change in total transport is the same for LR and HR. Figure 2 shows that the mean flow transports heat northward between 40° and 50°S for both models, and this transport is enhanced in the $2 \times \text{CO}_2$ runs by the stronger mean flow MOCs shown in Figs. 7a and 7b. South of 50°S , the stronger mean flow MOCs result in smaller southward heat transport by the mean flows. The southward eddy heat transport is reduced in the $2 \times \text{CO}_2$

simulation for both models between 30° and 45°S , which is where the LR eddy MOC in Fig. 7d is reduced. Across the ACC between 50° and 60°S , the eddy heat transport changes are much smaller than the mean transport changes. The change in eddy heat transport is about 0.03 PW, but of opposite signs for LR and HR. The LR runs have a very small standard deviation, so that the eddy transport increase is significant, and the LR with the GM parameterization does not match the sign of the HR eddy-resolving run eddy transport change. The HR

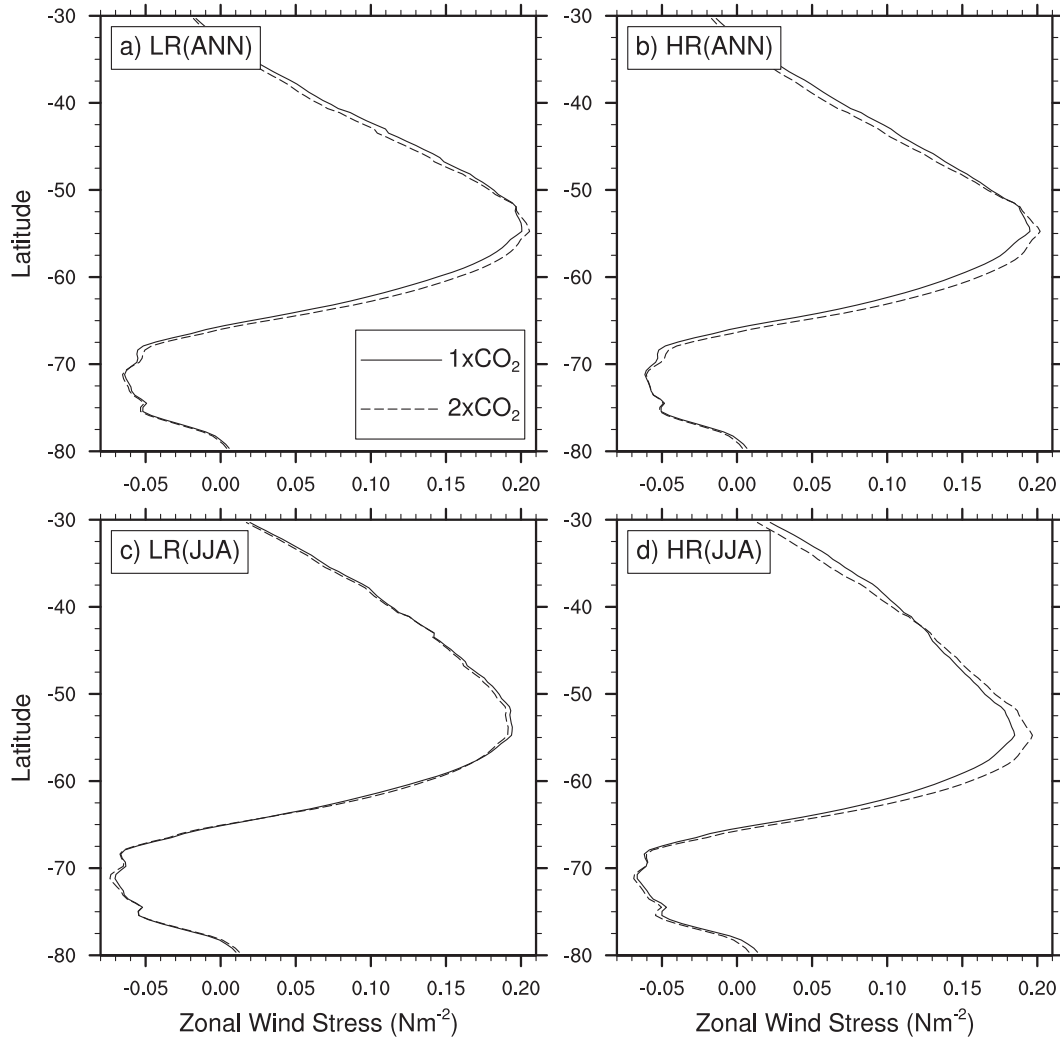


FIG. 6. The zonally averaged zonal wind stress (N m^{-2}) in $2 \times \text{CO}_2$ and $1 \times \text{CO}_2$ for the annual average in (a) LR and (b) HR, and the austral winter [June–August (JJA)] average for (c) LR and (d) HR.

reduction in eddy transport is barely significant but is a little surprising given that the HR wind stress shown in Fig. 6 has increased slightly. This result contrasts with zonal wind stress increase experiments using eddy-resolving models, such as Hogg et al. (2008), Screen et al. (2009), and Spence et al. (2010), which show that the southward eddy heat transport increases because of stronger eddy activity.

The mean heat transport can be further divided into components resulting from the zonally averaged flow, or overturning, and deviations from zonal-mean, or standing, eddies. Figure 5 of Volkov et al. (2010) shows that the northward heat transport due to the overturning is largely compensated by the southward heat transport of similar magnitude due to standing eddies. Our simulations show a similar compensation. Figure 10 shows

the change in overturning and standing eddy components of the mean heat transport between 30° and 80°S for LR and HR. For LR, the mean change is mostly as a result of the increased northward transport by the stronger overturning, which is only partially compensated by the increased standing eddy component across the ACC region (50° – 60°S). The HR increase in the overturning transport is slightly larger than in LR, because of the larger increase in zonal wind stress shown in Fig. 6. However, there is a larger difference between the increased transport by the standing eddies across the ACC, which in HR is nearly double that in LR. This is a result of the larger meridional velocities in meandering currents and covarying temperatures. For both LR and HR, the standing eddy transport increases by about 15%, which results in a

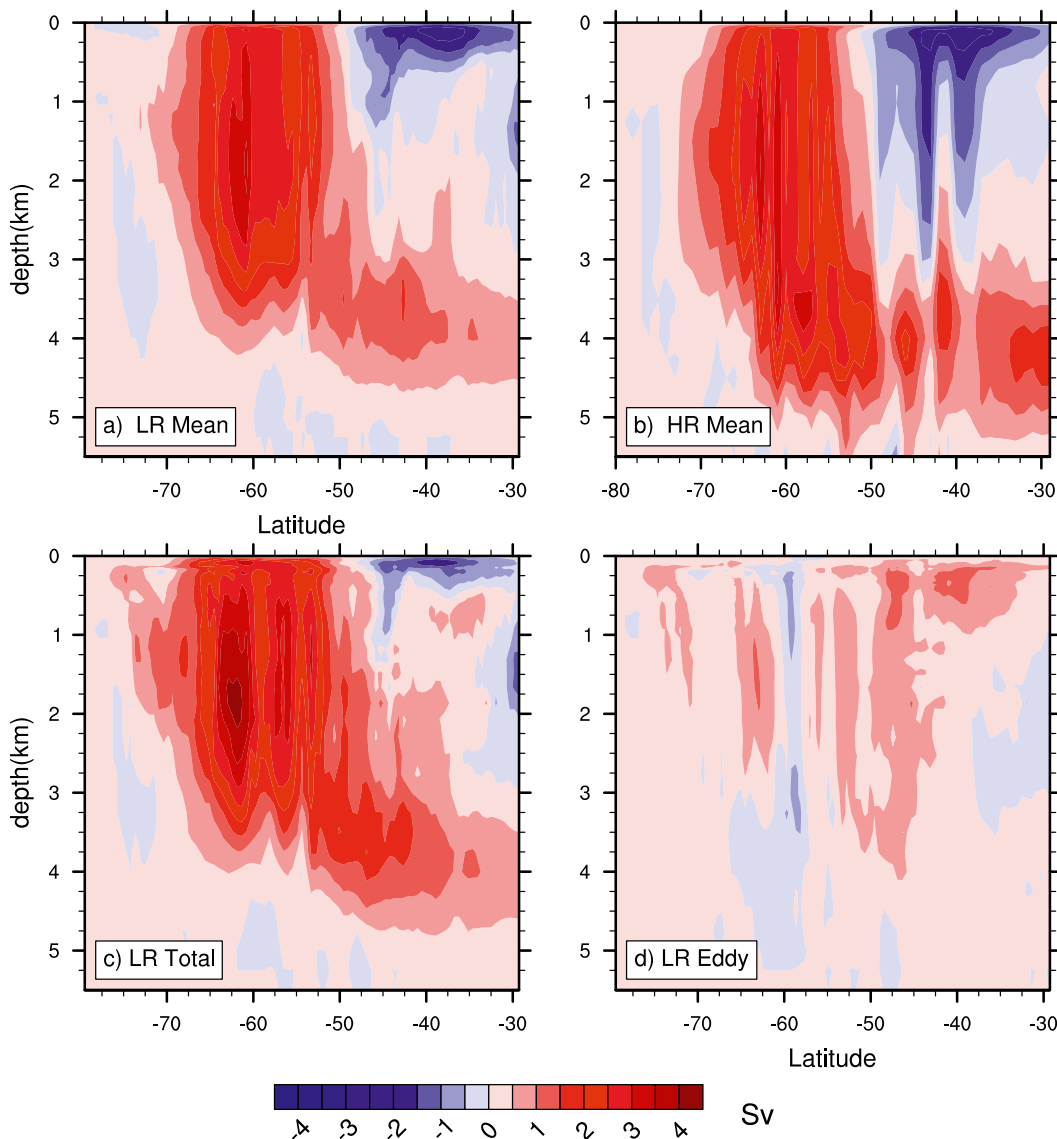


FIG. 7. Change in the mean flow MOC (Sv ; $1 \text{ Sv} \equiv 10^6 \text{ m}^3 \text{ s}^{-1}$) between $2 \times \text{CO}_2$ and $1 \times \text{CO}_2$ in (a) LR and (b) HR. For the LR model, the changes in (c) total flow MOC and (d) eddy flow MOC are also shown.

much stronger compensation of the overturning change in HR than in LR.

5. Discussion

The purpose of the runs documented in the last section is to determine whether the climate change response differs between a model where ocean eddies are parameterized and when they are resolved. In the ACC, mesoscale eddies are of leading-order importance, so this is a region upon which to concentrate. However, this question is not at all easy to answer because the control run climates of the two models are quite different. Figure 1 shows there is a considerable difference

in the Antarctic sea ice thickness distributions, and Table 1 shows the LR sea ice volume is 46% larger than HR. The different control run states can affect the $2 \times \text{CO}_2$ response around Antarctica and the ACC.

Bitz and Roe (2004) document the Arctic sea ice thickness changes in $1\% \text{ yr}^{-1}$ increasing CO_2 runs using three climate models, including the CCSM2. In all models the ice thickness decreases most where the control run ice is thickest, and they explain this result as a basic property of sea ice thermodynamics. Thinner ice conducts more heat through it than does thicker ice, which leads to greater heat loss and larger ice growth rates during the annual cycle for thin ice compared to thicker ice. In contrast, the changed ice melting rate is almost

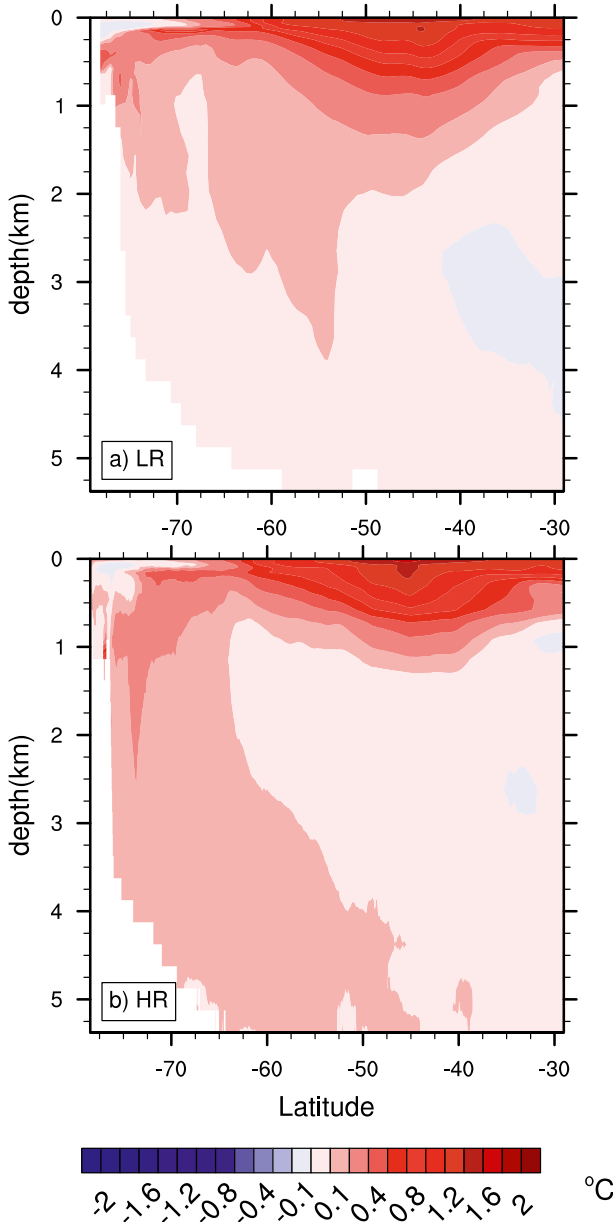


FIG. 8. Change in the zonally averaged ocean temperature ($^{\circ}\text{C}$) between $2 \times \text{CO}_2$ and $1 \times \text{CO}_2$ for (a) LR and (b) HR.

independent of the ice thickness, and only depends on the change in the radiative forcing. Thus, Bitz and Roe (2004) show that in a simple, analytic sea ice model the change in thickness needed so that the growth rate balances the increased melt rate due to $2 \times \text{CO}_2$ is smaller for thin ice than for thicker ice. In addition, they show that this simple model gives a good estimate of the Arctic sea ice thickness changes in the climate models, even where the control runs only have first-year ice and are ice free in summer. Bitz (2008) analyzes Arctic sea ice changes in the CMIP3 suite of climate models that

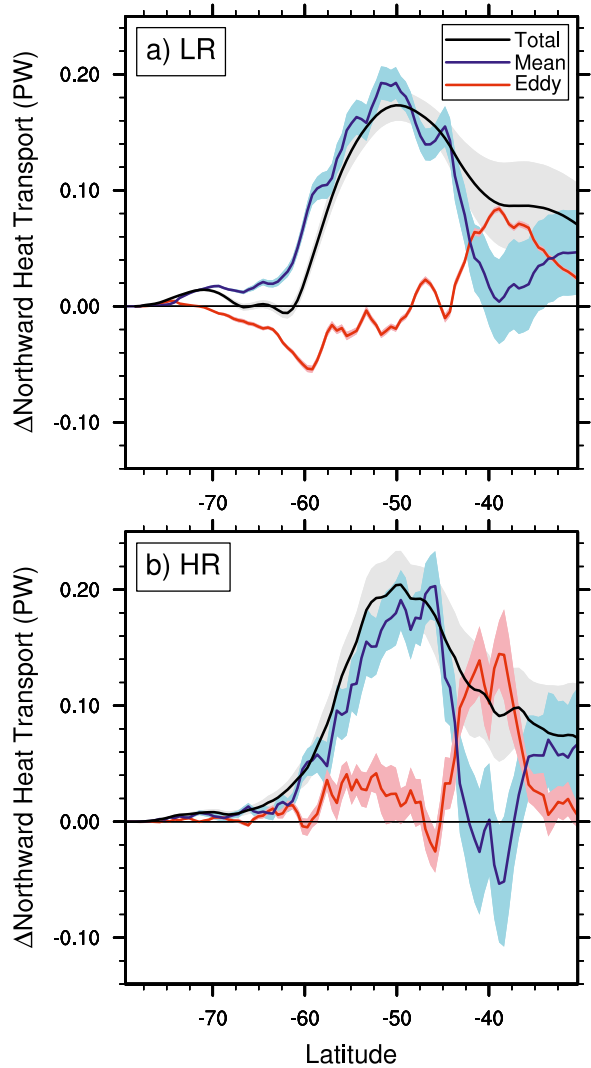


FIG. 9. Change between $2 \times \text{CO}_2$ and $1 \times \text{CO}_2$ in total northward ocean heat transport (PW) and its division into mean and eddy components for (a) LR and (b) HR. Shading indicates the standard deviation calculated as described in section 4.

includes CCSM3. She shows that when the models are forced by the same future climate scenario, those with the thickest control run ice distributions lose more ice than those with thinner control run distributions. Additional experiments with CCSM3 show that this result remains true even if the ice albedo feedback is turned off.

Both of the above studies focus on the Arctic, but are applicable to Antarctic sea ice because the results remain true for quite thin ice in control runs and to first-year ice. Comparison of Figs. 1 and 5 shows the ice thickness decreases most for both LR and HR exactly where the control run ice is thickest. The simplified model of Bitz and Roe (2004) suggests that the decrease in ice thickness is approximately quadratic in the original ice thickness.

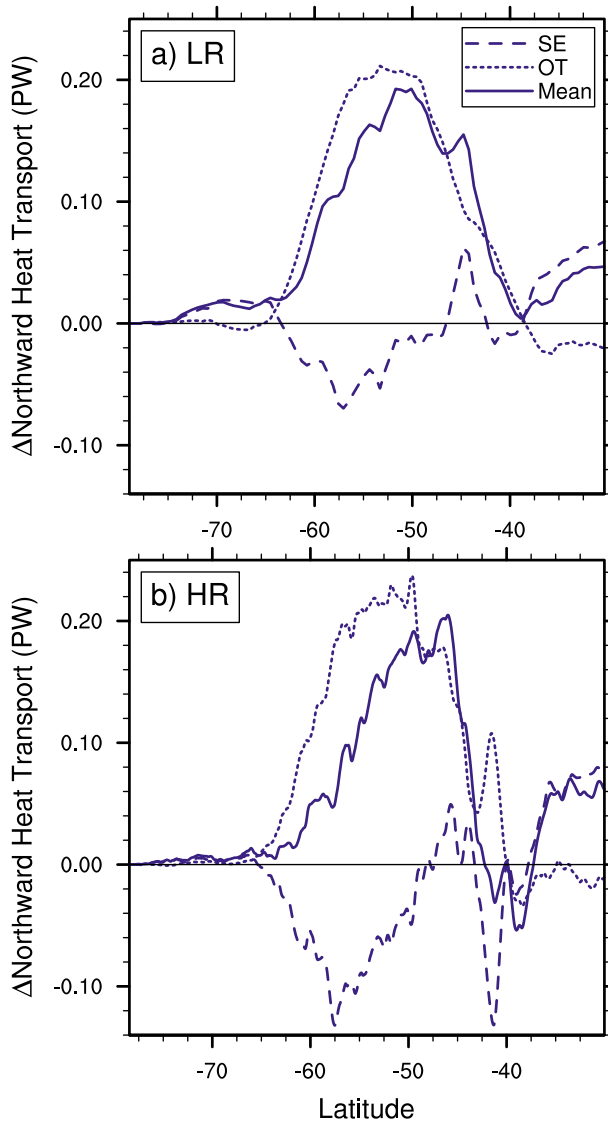


FIG. 10. Change between $2 \times \text{CO}_2$ and $1 \times \text{CO}_2$ in mean northward ocean heat transport (PW) and its division into overturning and standing eddy components for (a) LR and (b) HR.

The ratio of the LR to HR ice volume reductions from Table 1 is 2.15, which is very close to the square of the ratio of the control run ice volumes of 1.46. Also, Fig. 5 shows the larger LR ice loss occurs across the entire ice distribution, and is not the result of a larger reduction in LR sea ice extent. Therefore, the larger LR ice volume loss is mostly governed by the different control run ice thicknesses and, consequently, not by different changes in ocean-parameterized or -resolved eddy heat transport across the ACC toward the Antarctic sea ice in LR and HR.

Figure 3 shows there are larger areas off Antarctica for LR than HR where the surface temperature increase

for $2 \times \text{CO}_2$ is larger than 4°C . The areas are south of Africa and Australia and in the eastern Pacific. Comparison with Fig. 5 shows that these are the regions where the LR loses more ice than HR, especially in winter, and the differences in surface temperature and SST increases between LR and HR are larger and more circumpolar in winter than in other seasons. Thus, the meridional surface atmosphere temperature gradient across the ACC region for $2 \times \text{CO}_2$ is slightly weaker for LR than HR. This results in a weaker surface wind change for LR, and accounts for the smaller LR winter zonal wind stress change in Fig. 6. In turn, the different LR and HR winter wind stresses account for some of the different mean MOC responses shown in Figs. 7a and 7b. Therefore, many of the differences between the $2 \times \text{CO}_2$ responses for LR and HR are explainable by the different control run Antarctic sea ice distributions.

However, there are differences between LR and HR that are the direct result of parameterizing rather than resolving ocean mesoscale eddies. Figure 8 shows that the zonally averaged ocean temperature changes with $2 \times \text{CO}_2$ for LR and HR are very close in the upper ocean. But, there are differences in the deeper ocean both at midlatitudes and south of 62°S . Near Antarctica, more heat is carried down into the very deep ocean for HR. This is probably as a result of the 0.1° resolution in the sea ice component as well as the ocean component. Figure 9 shows that the very small changes in eddy heat transport across the ACC between 50° and 60°S are opposite in sign for LR and HR. The decrease in HR southward eddy heat transport is a little surprising, given that the zonal wind stress does increase slightly. Hogg et al. (2008), Screen et al. (2009), and Spence et al. (2010) report results from Southern Hemisphere zonal wind stress increase experiments using eddy-resolving ocean models, where the eddy transport increases to partially offset the increased northward heat transport by the mean flow. Gent and Danabasoglu (2011) show that these results can be mimicked in the CCSM4, which uses the same spatially dependent GM coefficient as the LR model in this work, although the degree of eddy compensation is not quite as large as in the eddy-resolving results. Note that zonal wind stress increases of at least 20%, and usually larger, are imposed in the referenced papers, in contrast to the very small $2 \times \text{CO}_2$ zonal wind stress increase shown in Fig. 6.

Figure 10 shows that the increased overturning northward heat transport in $2 \times \text{CO}_2$ across the ACC is comparable for LR and HR, but the compensating increase in southward heat transport due to standing eddies is twice as large for HR as in LR. Spence et al. (2012) show a comparable figure from two eddy-permitting ocean models in response to a large increase in Southern

Hemisphere zonal wind stress. Their Fig. 5 shows that the increase in standing eddy transport across the ACC is comparable to the overturning transport increase, similar to the HR. It also shows an increase in southward heat transport by transient eddies, in contrast to the HR decrease shown in Fig. 9b. Again, the imposed zonal wind stress increase in Spence et al. (2012) is more than one-third, in contrast to the very small increase shown in Fig. 6. Figure 10 illustrates the sensitivity of the standing eddy heat transport change to model resolution. The LR change is considerably smaller than the overturning transport change, so that the transient eddy heat transport component has to increase in order to compensate for the overturning flow increase. In HR, the change in the standing eddy component compensates for the overturning transport change, so that the transient eddy change can be small, and even the reduction in southward heat transport shown in Fig. 9b. In addition, all the referenced papers increase only the zonal wind stress and not the CO₂ level. In contrast, the change in HR eddy heat transport is affected by the temperature distribution change shown in Fig. 8b, as well as by the very small increase in zonal wind stress.

A similar transient eddy heat transport response was found by Bitz and Polvani (2012). They use the same LR and HR control runs as this work, and branch off 50-yr runs that have stratospheric ozone levels from the 1960s and 2000s. The response resulting from ozone depletion is similar to that from doubling CO₂: Antarctic sea ice is reduced, and Southern Ocean SSTs and mean flow MOCs are increased, as is the maximum zonal wind stress for both LR and HR. However, the sea ice loss percentages shown in their Fig. 1 are considerably smaller, about 25%–30% of those in Fig. 5 and Table 1 with $2 \times \text{CO}_2$ for both LR and HR. The ozone depletion produces a zonal wind stress increase across the ACC in both LR and HR, which results in an increased mean flow heat transport. However, Fig. 4d in Bitz and Polvani (2012) shows that the southward eddy heat transport is increased for LR but that there is almost no change in the HR eddy heat transport.

Previous work related to this study is a recent paper by Delworth et al. (2012), which compares control and $1\% \text{ yr}^{-1}$ increasing CO₂ runs in two GFDL climate models: CM2.1 and CM2.5. The CM2.1 ocean component has a resolution of 1° and uses an implementation of GM where the coefficient varies in the horizontal but not the vertical, and CM2.5 has a resolution of 0.25° and does not use a mesoscale eddy parameterization even though its resolution is eddy permitting rather than eddy resolving. However, in addition, CM2.1 and CM2.5 use different atmosphere and land components and different sea ice albedos in the control runs. In particular, the

atmosphere component resolution is 200 km in CM2.1 but 50 km in CM2.5, and CM2.5 has a larger equilibrium climate sensitivity than does CM2.1.

The Arctic sea ice is much thicker and more realistic in the CM2.5 control run than in CM2.1, and the Antarctic ice is also thicker in CM2.5, which is the opposite of the LR and HR control runs. Delworth et al. (2012) show that in the $2 \times \text{CO}_2$ run, CM2.5 has somewhat larger globally averaged surface temperature and ocean heat content increases than CM2.1, which can be attributed to its larger climate sensitivity. For LR and HR, these quantities are almost identical because both use the same atmosphere component, and so have the same equilibrium climate sensitivity. Figure 21 in Delworth et al. (2012) shows that the CM2.5 surface temperature increase in the high-latitude Southern Ocean is much larger than in CM2.1, in contrast to the similar values shown in Fig. 3. Their Fig. 22 shows much larger differences in the zonally averaged ocean temperature increase for $2 \times \text{CO}_2$ between CM2.1 and CM2.5 than between LR and HR in Fig. 8. CM2.5 has a larger temperature increase in the upper ocean, but a much smaller increase in the high-latitude deep Southern Ocean than does CM2.1. The deep ocean response is opposite in Fig. 8, where the HR moves more heat down near Antarctica than does LR. These differences between the GFDL models and CCSM3.5 used here are interesting, but the results are not directly comparable. The reason is that CM2.1 and CM2.5 have different atmosphere and land components, so the changes between these two models cannot be interpreted as just the effect of parameterizing, as opposed to partially resolving, ocean eddies.

Delworth et al. (2012) discuss the result that CM2.1 and CM2.4, which is the same as CM2.1 except the ocean component has 0.25° resolution, have different responses to greatly increased Southern Hemisphere winds. However, Farneti and Gent (2011) show that this is because the GM coefficient in CM2.1 is capped at $600 \text{ m}^2 \text{ s}^{-1}$, which is too small for the doubled zonal wind stress used. If the cap is raised to $1200 \text{ m}^2 \text{ s}^{-1}$, then the response to doubled Southern Hemisphere zonal wind stress for CM2.1 is quite similar to the response in CM2.4.

A companion paper in preparation, Bryan (2013, unpublished manuscript) analyzes the area-averaged ocean heat budget as a function of depth in the same four control and CO₂ transient forcing runs as are used in this work. Results show that the dominant heat balance at all depths in both the LR and HR control runs is between mean flow vertical advection that heats the ocean and eddy advection and mixing that cools it. Clearly, if the LR model does not use GM, then it cannot match the HR heat balance. In both the LR and HR $2 \times \text{CO}_2$ runs, the heating of the upper ocean is due to a similar

magnitude reduction in the eddy vertical advection rather than an increase in mean flow advection. Therefore, the upper-ocean heating rate for doubled CO_2 is very similar whether mesoscale eddies are parameterized or resolved.

6. Conclusions

The first conclusion from this work is that determining whether GM works well by comparing climate change responses is not at all straightforward because the LR and HR control runs have different climatologies, especially in their sea ice distributions. The different Arctic temperature responses in LR and HR are a direct result of the very different Arctic ice thickness distributions. The Antarctic sea ice volume for LR is 46% larger than HR, which mostly accounts for the significantly larger ice volume loss in LR for the $2 \times \text{CO}_2$ run. The different responses in high-latitude Southern Hemisphere surface atmosphere temperature and zonal wind stress can also be explained as a consequence of the different control run sea ice distributions.

The second conclusion is that there are differences in the LR and HR $2 \times \text{CO}_2$ runs that are a result of the GM parameterization not mimicking the HR results. Although the near-surface ocean temperature changes for LR and HR are very similar, the LR response does go deeper in the midlatitudes and not as deep at high latitudes as the HR response. Also, the LR mean flow MOC changes do not go as deep as the HR mean flow MOC changes. In addition, the very small changes in eddy heat transport across the ACC between the $2 \times \text{CO}_2$ and $1 \times \text{CO}_2$ runs have opposite signs for the LR and HR runs. This difference is partially explained by the different standing eddy contributions to the time mean heat transport that result from the different model resolutions, and not from the LR parameterization of transient eddies.

Climate models need to use a variable formulation for the GM coefficient, and not a constant coefficient, in order to get the correct response in the ACC region to changes in zonal wind stress (see Gent and Danabasoglu 2011; Farneti and Gent 2011). Further refinement of how the GM coefficient is specified as a function of ocean model variables might help reduce the differences seen in the LR and HR responses to the transient forcing of increasing CO_2 documented in this work.

Despite these differences between the LR and HR doubled CO_2 responses, this work, Bryan (2013, unpublished manuscript), and Bitz and Polvani (2012) all show that the GM parameterization in CCSM4 does a very good overall job of mimicking the resolved eddy climate change results. By “very good” we mean that the parameterization mimics the effects of mesoscale eddies not only qualitatively, but rather well quantitatively

over large spatial scales, such as the Atlantic, Pacific, and Indian sectors of the Southern Ocean. The LR runs do not reproduce all the small spatial features of the HR runs, but this cannot be expected of a parameterization. Therefore, we believe a third conclusion is that climate change results using a non-eddy-resolving ocean component with a modern GM formulation cannot be dismissed as unrealistic because the effects of eddies are parameterized rather than resolved.

A definitive answer to the original question of can Southern Ocean eddy effects be parameterized in climate models was clearly made rather difficult to ascertain by the different control run climatologies. Could the answer be reached more easily by a different approach? One possibility would be to run just the LR and HR ocean and sea ice components, starting from the same ice distributions and forced by atmosphere surface variables from the present HR 1% CO_2 simulation. This method would still have the drawbacks that the initial sea ice distribution would be inconsistent with the LR climatology, and changes because of the increased sea ice model resolution would not be separable from those because of the increased ocean model resolution. However, perhaps these forced ocean and sea ice component runs would be worth trying, instead of hoping that the next pair of LR and HR control run climatologies are nearly identical.

Acknowledgments. The authors thank Cecilia Bitz and Ryan Abernathey for illuminating discussions on sea ice and Southern Ocean dynamics, respectively. The control runs were completed under the auspices of the PetaApps project. All integrations were performed on the Kraken Cray XT5, which is located at the Oak Ridge National Laboratory and funded by the National Science Foundation. NCAR is also supported by the NSF.

REFERENCES

- Bitz, C. M., 2008: Some aspects of uncertainty in predicting sea ice thinning. *Arctic Sea Ice Decline: Observations, Projections, Mechanisms and Implications*, *Geophys. Monogr.*, Vol. 180, Amer. Geophys. Union, 63–76.
- , and G. H. Roe, 2004: A mechanism for the high rate of sea ice thinning in the Arctic Ocean. *J. Climate*, **17**, 3623–3632.
- , and L. M. Polvani, 2012: Antarctic climate response to stratospheric ozone depletion in a fine resolution ocean climate model. *Geophys. Res. Lett.*, **39**, L20705, doi:10.1029/2012GL053393.
- Bryan, F. O., M. W. Hecht, and R. D. Smith, 2007: Resolution convergence and sensitivity studies with North Atlantic circulation models. Part I: The western boundary current system. *Ocean Modell.*, **16**, 141–159.
- , R. Tomas, J. M. Dennis, D. B. Chelton, N. G. Loeb, and J. L. McClean, 2010: Frontal scale air–sea interaction in high-resolution coupled climate models. *J. Climate*, **23**, 6277–6291.

- Chelton, D. B., R. A. deSzoeke, M. G. Schlax, K. El Naggar, and N. Siwertz, 1998: Geographical variability of the first baroclinic Rossby radius of deformation. *J. Phys. Oceanogr.*, **28**, 433–460.
- Danabasoglu, G., and J. Marshall, 2007: Effects of vertical variations of thickness diffusivity in an ocean general circulation model. *Ocean Modell.*, **18**, 122–141.
- , R. Ferrari, and J. C. McWilliams, 2008: Sensitivity of an ocean general circulation model to a parameterization of near-surface eddy fluxes. *J. Climate*, **21**, 1192–1208.
- , S. Bates, B. Briegleb, M. Jochum, S. Jayne, W. Large, S. Peacock, and S. Yeager, 2012: The CCSM4 ocean component. *J. Climate*, **25**, 1361–1389.
- Delworth, T., and Coauthors, 2012: Simulated climate and climate change in the GFDL CM2.5 high-resolution coupled climate model. *J. Climate*, **25**, 2755–2781.
- Farneti, R., and P. R. Gent, 2011: The effects of the eddy-induced advection coefficient in a coarse-resolution coupled climate model. *Ocean Modell.*, **39**, 135–145.
- Gent, P. R., and J. C. McWilliams, 1990: Isopycnal mixing in ocean circulation models. *J. Phys. Oceanogr.*, **20**, 150–155.
- , and G. Danabasoglu, 2011: Response to increasing Southern Hemisphere winds in CCSM4. *J. Climate*, **24**, 4992–4998.
- , S. G. Yeager, R. B. Neale, S. Levis, and D. A. Bailey, 2010: Improvements in a half degree atmosphere/land version of the CCSM. *Climate Dyn.*, **34**, 819–833.
- , and Coauthors, 2011: The Community Climate System Model version 4. *J. Climate*, **24**, 4973–4991.
- Hallberg, R., and A. Gnanadesikan, 2006: The role of eddies in determining the structure and response of the wind-driven Southern Hemisphere overturning: Results from the Modeling Eddies in the Southern Ocean (MESO) project. *J. Phys. Oceanogr.*, **36**, 2232–2252.
- Hogg, A. M., M. P. Meredith, J. R. Blundell, and C. Wilson, 2008: Eddy heat flux in the Southern Ocean: Response to variable wind forcing. *J. Climate*, **21**, 608–620.
- Holland, M. M., D. A. Bailey, B. P. Briegleb, B. Light, and E. C. Hunke, 2012: Improved sea ice shortwave radiation physics in CCSM4: The impact of melt ponds and aerosols on Arctic sea ice. *J. Climate*, **25**, 1413–1430.
- Kirtman, B. P., and Coauthors, 2012: Impact of ocean model resolution on CCSM climate simulations. *Climate Dyn.*, **39**, 1303–1328.
- Lin, S. J., 2004: A “vertically Lagrangian” finite-volume dynamical core for global models. *Mon. Wea. Rev.*, **132**, 2293–2307.
- Lipscomb, W. H., E. C. Hunke, W. Maslowski, and J. Jakacki, 2007: Ridging, strength, and stability in high-resolution sea ice models. *J. Geophys. Res.*, **112**, C03S91, doi:10.1029/2005JC003355.
- Mahlstein, I., and R. Knutti, 2011: Ocean heat transport as a cause for model uncertainty in projected Arctic warming. *J. Climate*, **24**, 1451–1460.
- Maltrud, M., F. O. Bryan, and S. Peacock, 2010: Boundary impulse response functions in a century-long eddying global ocean simulation. *Environ. Fluid Mech.*, **10**, 275–295.
- Marshall, J., and K. Speer, 2012: Closure of the meridional overturning circulation through Southern Ocean upwelling. *Nat. Geosci.*, **5**, 171–180.
- McClellan, J. L., and Coauthors, 2011: A prototype two-decade fully coupled fine-resolution CCSM simulation. *Ocean Modell.*, **39**, 10–30.
- Neale, R. B., J. H. Richter, and M. Jochum, 2008: The impact of convection on ENSO: From a delayed oscillator to a series of events. *J. Climate*, **21**, 5904–5924.
- Oleson, K. W., and Coauthors, 2008: Improvements to the Community Land Model and their impact on the hydrological cycle. *J. Geophys. Res.*, **113**, G02021, doi:10.1029/2007JG000563.
- Screen, J. A., N. P. Gillett, D. P. Stevens, G. J. Marshall, and H. K. Roscoe, 2009: The role of eddies in the Southern Ocean temperature response to the southern annular mode. *J. Climate*, **22**, 806–818.
- Smith, R. D., M. E. Maltrud, F. O. Bryan, and M. W. Hecht, 2000: Numerical simulation of the North Atlantic Ocean at 1/10°. *J. Phys. Oceanogr.*, **30**, 1532–1561.
- Soloviev, M., P. H. Stone, and P. Malanotte-Rizzoli, 2002: Assessment of mesoscale eddy parameterizations for a single-basin coarse-resolution ocean model. *J. Geophys. Res.*, **107**, 3126, doi:10.1029/2001JC001032.
- Spence, P., J. C. Fyfe, A. Montenegro, and A. J. Weaver, 2010: Southern Ocean response to strengthening winds in an eddy-permitting global climate model. *J. Climate*, **23**, 5332–5343.
- , O. A. Saenko, C. O. Dufour, J. L. Sommer, and M. H. England, 2012: Mechanisms maintaining Southern Ocean meridional heat transport under projected wind forcing. *J. Phys. Oceanogr.*, **42**, 1923–1931.
- Volkov, D. L., L.-L. Fu, and T. Lee, 2010: Mechanisms of the meridional heat transport in the Southern Ocean. *Ocean Dyn.*, **60**, 791–801.
- Wilks, D. S., 1995: *Statistical Methods in the Atmospheric Sciences*. International Geophysics Series, Vol. 59, Academic Press, 467 pp.